Theor. Appl. Climatol. 69, 199–212 (2001)

Theoretical and Applied Climatology

[1] GKSS Research Center, Geesthacht, Germany
[2] University College Cork, Cork, Ireland

Evaluation of the hydrological components added to an atmospheric land-surface scheme

H.-T. Mengelkamp[1], **G. Kiely**[2], and **K. Warrach**[1]

With 9 Figures

Received October 25, 2000
Revised February 16, 2001

Summary

Discharge from a small grassland catchment in Ireland is simulated with the atmospheric land-surface scheme SEWAB. Hydrological processes are parameterized to represent surface runoff and baseflow generation and soil moisture storage changes. Surface ponding and infiltration are explicitly described in order to account for the rapid response of streamflow to precipitation events. The annual discharge, the evapotranspiration and individual flood flows are accurately modelled. The simulation of soil moisture at various depths is close to the observations from time domain reflectometer measurements. An analysis of the significance of individual hydrological processes for discharge simulation from the small catchment found the ponding process to be essential for time periods of less than 12 hours. A depth dependent saturation hydraulic conductivity improves the simulations on all time scales.

1. Introduction

A fundamental difficulty in evaluating surface hydrological processes in an atmospheric land-surface scheme (LSS) arises from a scale mismatch of available observations. We define the surface water balance as the water balance of a soil column down to the bottom of the soil model, including the water on the surface and in the interception reservoir:

$$P - E - dS/dt = R \tag{1}$$

Precipitation P, evapotranspiration E and the change in soil moisture storage dS/dt are measured by micrometeorological methods at plot scale. At this scale measurements of runoff R are usually not available. Runoff is the excess water per surface unit calculated as the excess of precipitation over evapotranspiration and local moisture storage change. In hydrological terms this is "runoff generation" or "effective precipitation" (Graham et al., 2000). Runoff is an instantaneous value without translation or transformation by storage or transport processes. The observable variable to compare simulated runoff with is streamflow, which is measured at gauging stations in a river channel system. Streamflow represents a regional or larger scale catchment area. A routing model is needed to translate runoff into streamflow. Because of this scale distinction, evapotranspiration and runoff are commonly not validated simultaneously, although they are interdependent.

There are two major difficulties in using streamflow to validate the runoff generation process in a LSS. Firstly, the routing model needs calibration to adequately describe the horizontal water movement in a catchment. This calibration may compensate for errors in the simulated runoff. Secondly, inhomogeneous soil and vegetation characteristics and forcing data cause an inaccurate determination by simulations as well as measurements of P, E and dS/dt on catchment scale.

Our study focuses on the local scale. We had streamflow data available from a very small catchment, which can be considered homogeneous with respect to vegetation cover, soil type and atmospheric forcing. Application of a routing model is not suitable for such a small catchment. However, calibration of the parameterization schemes for horizontal water transport processes is still required for temporal scales smaller than the typical residence time of water in the catchment. Surface ponding and baseflow storage are included to account for horizontal water movement.

In a General Circulation Model (GCM) Hagemann and Dümenil (1999) represent the lateral waterflow by single linear reservoirs for overland flow and baseflow, respectively, and a cascade of equal linear reservoirs for riverflow. Lohmann et al. (1996), Habets et al. (1999), Lobmeyr et al. (1999) and Benoit et al. (2000) coupled an atmospheric land-surface scheme and a horizontal routing scheme in order to study the surface water budget on catchment scale. The grid size of their models ranges from about 10 to 400 km^2. The horizontal water flow is separated into the transformation inside a grid box and the flow in the river channel system. All these studies aim at calculating streamflow on a daily basis and corresponding large spatial scales. On the mesoscale Mölders and Raabe (1997) coupled a hydrological model to an atmospheric mesoscale model and found that surface hydrology influences cloud and rainfall formation on the regional scale even in a 24 hour simulation. No attempt, however, was made to validate runoff generation.

The Project for Intercomparison of Land-surface Parameterization Schemes (PILPS) focuses on evaluating and improving land-surface schemes for climate and weather prediction models (Hendersen-Sellers et al., 1995). An intercomparison of model simulated runoff for the site of the Cabauw micrometeorological tower in the Netherlands (PILPS phase 2a, Chen et al., 1997) showed a large variation among the participating land-surface schemes even on an annual time scale. This local scale study was followed by a regional-scale experiment, with a focus on the surface energy and water balance in the Arkansas-Red-River basin (PILPS phase 2c, Wood et al., 1998). To compare runoff with streamflow a routing scheme was applied to transport runoff into, and through, the river channel system to gauging stations (Lohmann et al., 1998). Considerable differences were found among the participating schemes in the spatial pattern of mean annual runoff and the timing of selected hydrographs, although the same routing scheme was used for all models. Koster and Milly (1997) investigated the consequences of different evaporation and runoff formulations in several land-surface schemes. They conclude that "if the formulation of runoff in a land-surface scheme (LSS) is poor, the LSS will produce unrealistic annual evaporation rates regardless of the quality of the evaporation formulation" (Koster et al., 2000).

Often only evapotranspiration and the sensible heat flux were subject of validation experiments for 1-dimensional LSS with no attention paid to runoff (e.g. Chen et al., 1997; Noilhan and Planton, 1989). This study focuses on the validation of the runoff generation process using streamflow data, which represents the same spatial and temporal scale as evaporation measurements.

The land-surface scheme SEWAB (Surface Energy and Water Balance, Mengelkamp et al., 1999) solves the coupled surface energy and water balance equations and simulates the vertical heat and water fluxes within the soil. Since its participation in PILPS phases 2a and 2c SEWAB runoff calculation for large-scale applications has been improved. A variable infiltration capacity is included for surface runoff generation (Warrach et al., 1999) and storage compartments are added to account for the fast and slow baseflow component, respectively (Mengelkamp et al., 2000). In this paper we attempt to simulate streamflow from a small catchment which can be considered a plot scale area. The time step is 20 min. These scales are similar to the scales being represented by surface measurements of the remaining components of the surface water and energy balance.

The paper is organized as follows. The parameterization schemes for the surface water balance components are described in section 2. The field site is described in section 3. Section 4 outlines the parameters describing the site characteristics and the model calibration procedure. The simulation of surface water components and temperatures is discussed in section 5, while the significance of single hydrological processes is investigated in section 6. A summary is given in section 7.

2. Hydrological components of SEWAB

2.1 The surface water balance

The land-surface scheme SEWAB solves the coupled system of the surface energy and water balance equations. The energy balance components are parameterized in a way similar to the land-surface schemes of Noilhan and Planton (1989) and Deardorff (1978) and described in detail by Mengelkamp et al. (1999). In this paper we focus on the hydrological components of the soil-surface processes (Fig. 1).

In Eq. (1) the evapotranspiration $E[\mathrm{kg\,m^{-2}\,s^{-1}}]$ includes transpiration and evaporation from the interception reservoir and bare soils. $R[\mathrm{kg\,m^{-2}\,s^{-1}}]$ represents runoff which comprises surface runoff, subsurface runoff and baseflow. $dS[\mathrm{kg\,m^{-2}}]$ is the change in soil moisture storage during a time interval $dt[s]$. Storage of water in the interception reservoir and on the surface as ponded water are included in the storage term. In the annual water balance the change in storage is assumed negligible but on time scales smaller than 1 year changes in all storage components are taken into account. Precipitation as an external forcing parameter is provided from measurements for off-line simulations. In this study precipitation measurements at 20 minute intervals are used.

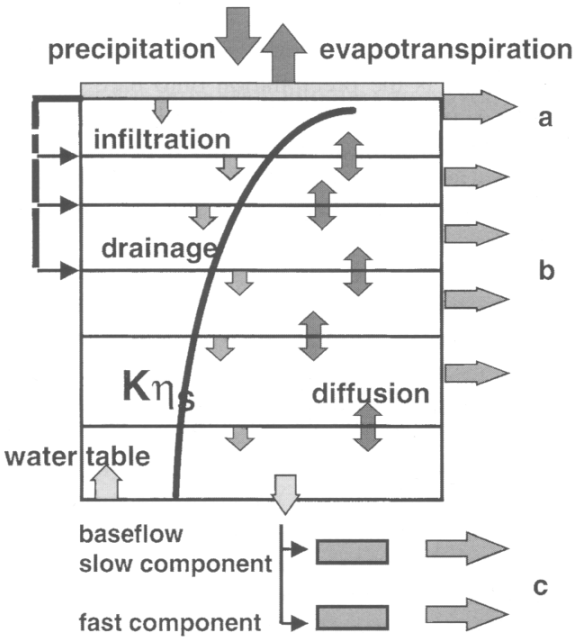

Fig. 1. Hydrological components of the land surface scheme SEWAB. a, b and c represent overland surface runoff, subsurface runoff and baseflow, respectively

2.2 Evapotranspiration

The evapotranspiration is formulated from Noilhan and Planton (1989) as the sum of the evaporation from bare soil E_g and the wet foliage E_r and the transpiration from the dry part E_{tr}:

$$E = E_g + \delta_w E_r + (1 - \delta_w) E_{tr} \tag{2}$$

A detailed description of the formulation of E_g, E_r and E_{tr} is given in Mengelkamp et al. (1999). The fraction of the foliage surface coated with moisture δ_w is formulated as a function of the maximum interception reservoir (Deardorff, 1978) which depends on the leaf area index LAI being assumed to vary seasonally. For this study there is no bare soil and $E_g = 0$.

The stomatal resistance R_S is described as

$$R_S = \frac{R_{S\min}}{LAI} F_1 F_2^{-1} F_3^{-1} F_4^{-4} \tag{3}$$

with the factor F_1 describing the influence of the photosynthetically active radiation (Dickinson, 1984)

$$F_1 = \frac{1 + f}{f + \frac{R_{S\min}}{R_{S\max}}} \tag{4}$$

with $f = 0.55\,(R_G/R_{GL})(2/LAI)$ where R_{GL} is a limiting value depending on vegetation type and set to 90. R_G is the incoming solar radiation. A minimum stomatal resistance of $80\,\mathrm{s\,m^{-1}}$ according to literature data for grassland (Peters-Lidard et al., 1997) and a maximum value of $1000\,\mathrm{s\,m^{-1}}$ are assumed.

The factors F_2, F_3 and F_4 take into account the effect of water stress, the effect of water vapor deficit and the air temperature dependence on the surface resistance, respectively (Noilhan and Planton, 1989).

2.3 Diffusion, drainage and vertical redistribution of water

The vertical diffusion of water in the soil is described by Richards equation for unsaturated flow in porous media:

$$\frac{\partial \eta}{\partial t} = -\frac{\partial}{\partial z}\left(D_\eta \frac{\partial \eta}{\partial z} + K_\eta\right) \tag{5}$$

where $\eta[\mathrm{m^3\,m^{-3}}]$ is the soil moisture content, $D_\eta[\mathrm{m^2\,s^{-1}}]$ the hydraulic diffusivity and $K_\eta[\mathrm{m\,s^{-1}}]$ the hydraulic conductivity.

The functional relationships between the soil moisture potential Ψ_η, D_η and K_η represent the soil moisture characteristic curves (Clapp and Hornberger, 1978). The hysteresis effect, stating that the equilibrium soil wetness at a given suction is greater in the drying than in the wetting phase (Hillel, 1982) is neglected here as well as any influence of temperature on the moisture transport and vice versa.

As the soil moisture characteristics (hydraulic diffusivity, conductivity and soil moisture potential) change exponentially with soil moisture, and in order to avoid excessively small time steps due to the very thin uppermost layer, Eq. (5) is solved by the semi-implicit Thomas-algorithm of Richtmyer and Morton (1967). At the upper boundary, the soil moisture of the uppermost layer is updated every time step according to the difference between infiltration, evaporation and runoff out of this layer. At the lower boundary only gravitational drainage is allowed. The gravitational drainage term of Eq. (5)

$$\frac{\partial \eta}{\partial t} = -\frac{\partial K_\eta}{\partial z} \tag{6}$$

is calculated explicitly.

A depth dependent saturation hydraulic conductivity after Beven (1984) is included to account for a vertically varying pore size:

$$K_{\eta S} = K_{\eta S0} \exp(-fz) \tag{7}$$

The non-dimensional parameter f is supposed to vary between 1 and $13\,\mathrm{m^{-1}}$ according to soil characteristics. $K_{\eta S0}$ is the saturation hydraulic conductivity at the surface (see Fig. 1).

To avoid negative η-values for large time steps in Eq. (6) Bonan (1996) applied partial time steps for $\Delta t > 10\,\mathrm{min}$ adjusting K_η to decreasing η values. We use a simpler approach in order to save simulation time by multiplying the right hand side of Eq. (6) by a factor equal to $0.5+(1-(\eta/\eta_s)^4)$. This factor which is found by trial and error reduces the drainage term for large η and K_η values.

Any soil water in excess of saturation is partitioned into one part being redistributed successively to the soil layer above and a second part which contributes to horizontal runoff. In each layer, the partitioning between water going to storage and water going to runoff is achieved through calibration. The redistribution of water simulates a rising ground water table.

2.4 Ponding, infiltration and surface runoff

The Variable Infiltration Capacity approach (VIC approach, Wood et al., 1992) was initially used for this small Irish catchment and was found unsatisfactory. The VIC scheme allows runoff generation before total saturation of the uppermost layer of the model grid box. The opposite effect, namely delayed runoff generation after saturation of the soil, was found to occur during heavier rainfall events over the small field site. Surface water accumulates above the soil column when the rainfall rate exceeds the rate of infiltration. This ponded water forms surface runoff in a delayed mode. If the allowable height of the ponding storage, $h_0^{\max}$, is exceeded the excess water instantaneously forms runoff.

With h_0^n being the height of the ponding storage at time step n the maximum infiltration rate $I_{\max}$ (the total amount of available water to infiltrate per time step) is

$$I_{\max} = \frac{h_0}{\Delta t} + P(1-veg) + R_{ld} \tag{8}$$

veg denotes the fraction of vegetation and $P(1-veg)$ is the precipitation onto bare ground ($veg = 1$ in this study). R_{ld} describes leaf drip. The potential infiltration rate I_{pot} depends on the soil moisture characteristics of the uppermost soil layer with thickness Δz_1 (Mahrt and Pan, 1984):

$$I_{pot} = K_{\eta_s} + D_{\eta_s} \frac{(\eta_s - \eta_1)2}{\Delta z_1} \tag{9}$$

The actual potential infiltration rate I_{pot_a} is the minimum of I_{pot} and the amount of water which can occupy the empty pore space:

$$I_{pot_a} = \min\left[I_{pot}, \frac{(\eta_s - \eta_1)\Delta z_1}{\Delta t}\right] \tag{10}$$

The actual infiltration rate is

$$I_{act} = \min[I_{pot_a}, I_{\max}] \tag{11}$$

The difference between the total amount of water falling onto the ground and the actual infiltration

rate is added to the ponding storage

$$h_0^{n+1} = h_0^n + \left[\frac{P(1-veg) + R_{ld}}{\rho_w} - I_{act}\right]\Delta t \quad (12)$$

Discharge from the ponding storage is assumed to depend linearly on the amount of water in the ponding storage and is formulated after Hall (1968):

$$R_{pond}^{n+1} = \frac{\ln 2}{T_{pond}} h_0^{n+1} \rho_w \quad (13)$$

The recession coefficient $(\ln 2/T_{pond})$ describes the outflow behaviour. The time constant T_{pond} is the decay time by which the amount of water in the ponding storage reduces to 50 percent of saturation. Discharge at the surface comprises R_{pond} and any amount of rain in excess of the maximum ponding storage capacity.

2.5 Subsurface runoff and baseflow

A linearly increasing outflow between field capacity and saturation is applied to the subsurface soil layers. Subsurface runoff is formulated similar to the ARNO model conceptualization which is widely used for baseflow generation processes (Francini and Pacciani, 1991; Dümenil and Todini, 1992). Below saturation, runoff from these layers follows Eq. (14). The outflow rate of any layer k is proportional to the current soil water storage in that layer:

$$R_{S_k} = \frac{\ln 2}{T_{h_k}} \eta_k \Delta z \rho_w \quad (14)$$

where the half life T_{h_k} is the time for subsurface flow to recede to 50 percent of saturation from an initially saturated state and is determined by calibration. As the response time of surface runoff to rainfall events is much smaller than the response of subsurface flow, T_{h_k} is much larger than T_{pond}. Any water in excess of saturation is added to runoff.

The baseflow component of runoff is modelled using two linear groundwater storages with a slow and a fast component, respectively (see Fig. 1). These storages are filled by Darcian flow R_D from the lowest soil layer. The non-dimensional parameter $0 \leq \gamma \leq 1$ partitions the water entering the two storages. Runoff $R_{s/f}$[kg m^{-2} s^{-1}] and stored water $S_{s/f}^t$[kg m^{-2}] of the slow (s) and fast (f) storage at time step t are calculated as

$$R_{s/f}^t = MIN\left[\frac{\ln(2)}{T_{s/f}}(S_{s/f}^{t-\Delta t} + \gamma R_D \Delta t), \frac{S_{s/f}^{t-\Delta t} + \gamma R_D \Delta t}{\Delta t}\right] \quad (15)$$

$$S_{s/f}^t = S_{s/f}^{t-\Delta t} + (\gamma R_D - R_{s/f})\Delta t \quad (16)$$

For the fast component γ is replaced by $(1-\gamma)$. T and γ are used as calibration parameters. Parameter values used in this study are given in section 4.

3. The field site

The research area is sited near Donoughmore, 25 km Northwest of Cork, in the south of Ireland. It encompasses a 14.5 ha grassland subcatchment (about 300×480 m^2, elevation 210 m amsl) of the Dripsey catchment which is in turn a subcatchment of the river Lee watershed. Runoff from the site drains to a small stream where the flow is monitored at a capital notch weir. The site is agricultural grassland, typical of the landuse and vegetation in this part of the country. The grassland type can be described as high, and moderately high, quality pasture and meadow. The grass height varies from a low of 5 cm to a high of about 40 cm. The grass is cut about three times per year. The bedrock at about 2 m to 4 m depth is Devonian Sandstone. The soil profile is characterised by a top 5 cm humus layer overlying a dark brown A horizon of sand texture to a depth of 20 cm. The yellowish-brown B horizon of sand texture grades into a brown gravely sand parent material at about 30 cm. The site is gently sloping at about 4 percent grade to a stream.

The climate is temperate and humid and influenced by the warm Gulf Stream of the North East Atlantic. Mean annual precipitation in the Cork region is about 1100 mm. The rainfall regime is characterised by long duration events of variable intensity which occur at any time of the year. Short duration, high intensity events, occur mainly in summer (Kiely et al., 1998). Over the 12 month study period the maximum daily rainfall was 75 mm on August 3, 1997 and the peak hourly intensity was 11.6 mm on August 26, 1997.

The field instrumentation comprises nine water content time domain reflectometers (TDRs) spread out over the field site over a depth of 60 cm, a rain gauge, a class A evaporation pan, a stream water level recorder, and an automatic weather station including net radiometer, air temperature, relative humidity, barometric pressure, surface temperature, soil temperature, soil heat flux plates, wind speed and wind direction. Data is recorded continuously at 20 minute intervals. In this study, data from the period July 1, 1997 to June 30, 1998 are used. Streamflow is used to calibrate the model. Soil temperature at 4 cm depth, surface temperature and soil moisture readings at 7 depth points from 2 cm to 60 cm depth are used for validation purposes.

4. Model set up, data availability and calibration

4.1 Model configuration

The 1-dimensional SEWAB represents the entire catchment. The model soil column is partitioned into eight soil layers with increasing thickness from 4 cm (close to the surface) to 20 cm for the bottom layer which is centered at 1.14 m depth (Fig. 2). Based on site inspections we assume 35 percent of the roots in the first layer, 40 percent in the second and 25 percent in the third one. Transpiration water is extracted from these three layers only.

Conceptually the model is not able to describe the soil layering appropriate for the actual soil profile described in section 3. The soil parameters correspond to a mixture of sand and clay soil. In situ measurements of the saturated hydraulic conductivity ranged from $1.7 \cdot 10^{-6}\,\mathrm{m\,s^{-1}}$ to $3.2 \cdot 10^{-6}\,\mathrm{m\,s^{-1}}$. In the model we use $2.0 \cdot 10^{-6}\,\mathrm{m\,s^{-1}}$ for the surface saturated hydraulic conductivity and applied equation (7) with $f = 6$ for the remaining layers. The saturated volumetric water content is $0.452\,\mathrm{m^3\,m^{-3}}$, the moisture potential -0.4 m and the wilting point is assumed at $0.18\,\mathrm{m^3\,m^{-3}}$. The field capacity is $0.34\,\mathrm{m^3\,m^{-3}}$ and the non-dimensional pore size distribution b in the Clapp and Hornberger (1978) relations is 11.4. The thermal diffusivity and the heat capacity are $8.4 \cdot 10^{-7}\,\mathrm{m^2\,s^{-1}}$ and $2.1 \cdot 10^{6}\,\mathrm{J\,m^{-3}\,K^{-1}}$, respectively (values for these parameters can be found e.g. in Stull (1988)).

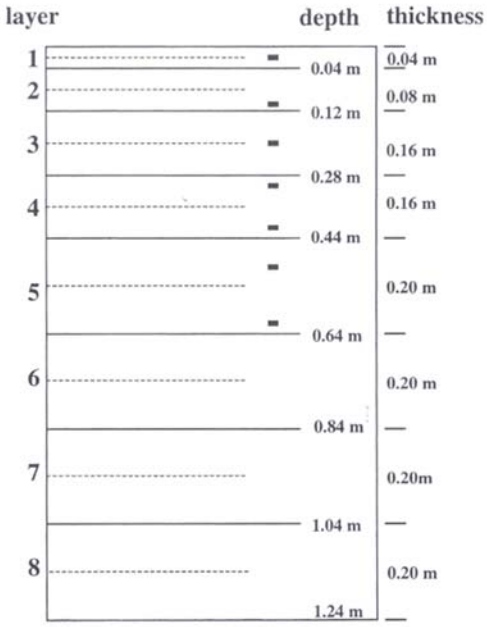

Fig. 2. Vertical grid configuration of the soil model. The black squares indicate the depth of the soil moisture measurements

Vegetation parameters representative for agricultural grassland are used. During the growing season the grass increases to a height of approximately 40 cm before it is harvested. We neglect these short term changes, but prescribe a seasonal cycle for the leaf area index with the minimum of 1 in January and a maximum of 3.2 in July. For the totally vegetated grassland catchment the roughness length was estimated to 0.02 m, the emissivity is 0.95 and the albedo 0.25.

The model is run with a time step of 20 min corresponding to the averaging period of the observations. Soil temperature is initially set uniformly to 286 K which is the observed surface temperature while the soil moisture initially is assumed to be saturated at the bottom varying linearly to $0.8\,\eta_s$ at the surface. The soil moisture at the bottom is fixed at its saturation value. At the lower boundary a seasonal cycle is prescribed for the soil temperature with a mean value of 283 K and an amplitude of 6 degrees.

4.2 Data availability and calibration

Forcing data and streamflow data were available from July 1, 1997 to June 30, 1998. The first half of this time series until December 31, 1997 is used for calibration, the second half for validation. Additional data sets comprise measurements by an evaporation pan from July 1 to September 31, 1997, measurements of soil moisture content in seven depths from February 20 to June 30, 1998 and surface temperature measurements by an infrared transducer during the period November 13–30, 1997.

The parameterization schemes for the surface atmosphere exchange processes require no calibration once the appropriate vegetation and soil parameters are fixed. The vegetation parameters were checked by inspection of the annual water balance which justifies the assumption of a vanishing soil moisture storage change as described in the next section. The transformation of model generated runoff to streamflow includes the highly complex processes of water storage and water transport. For temporal scales less than the residence time, these processes can only be adequately simulated through calibration for the particular watershed. In this study the transformation is simulated through ponded water and groundwater storages and adjusting their respective time constants.

With the soil and vegetation parameters left unchanged, the hydrological processes are calibrated comparing the measured and simulated time series of streamflow for the period July 1 to December 31, 1997. Calibration is performed by tuning the appropriate parameters manually. The baseflow component is adapted by varying the time constants of the fast and slow storage compartment, respectively. The factor which partitions the drainage flow from the lowest soil layer into the two storage compartments is fixed at $\gamma = 0.5$. Previous experience has shown that results are insensitive to this parameter except if it is close to 0 or 1. Time constants of 0.3 days and 4 days for the fast and slow storage, respectively, are found to describe the baseflow component acceptably. Surface runoff is calibrated by adjusting the maximum ponding height ($h_0^{\max} = 0.03\,\mathrm{m}$), the time constant for the ponding storage ($T_{pond} = 0.25\,\mathrm{days}$) and the time constant for the uppermost soil layer ($T_{h_1} = 15\,\mathrm{days}$). From the intermediate layers only little runoff is allowed through a time constant of 300 days. Streamflow is most sensitive to 4 out of the 7 calibration parameters, namely the time constants for the ponding storage and the two baseflow compartements as well as to the maximum ponding height. Because surface runoff and baseflow are calibrated separately, effectively only 2 parameters had to be adjusted at a time.

4.3 The annual water balance

Except for the saturation hydraulic conductivity, which is taken from measurements, all parameters describing soil and vegetation characteristics are literature data (e.g. Stull (1988) and Peters-Lidard et al., 1997). Whether their combination is appropriate to simulate the surface water balance reasonably well is evaluated by considering the annual means. It is assumed that the soil moisture storage is the same at the beginning and the end of the experimental period. Table 1 summarizes the annual water balance components. Because precipitation is input to the model the concurrence of observed and simulated streamflow indicates a fair simulation of the evapotranspiration on an annual time scale. The change in soil moisture storage is small, as required.

From time series statistics over more than 50 years Kiely (1999) found a mean annual precipitation range of 1000–1400 $\mathrm{kg\,m^{-2}}$ for the western part of Ireland and about 700 $\mathrm{kg\,m^{-2}}$ for the east. Compared to this, our investigation period shows above average precipitation. Roughly a quarter of the total precipitation is transported back to the atmosphere through evapotranspiration and 3/4 goes into runoff. Only about one percent

Table 1. The annual surface water balance components for the period July 1, 1997 to June 30, 1998, all units are in $\mathrm{kg\,m^{-2}}$

Element	Observed	Simulated
Precipitation	**1617**	**1617**
Total river runoff	**1239**	**1208**
Surface runoff		408
Baseflow		800
Evapotranspiration	(378)	**388**
Intercep. evaporation		119
Transpiration		269
Change in soil moisture storage		**21**

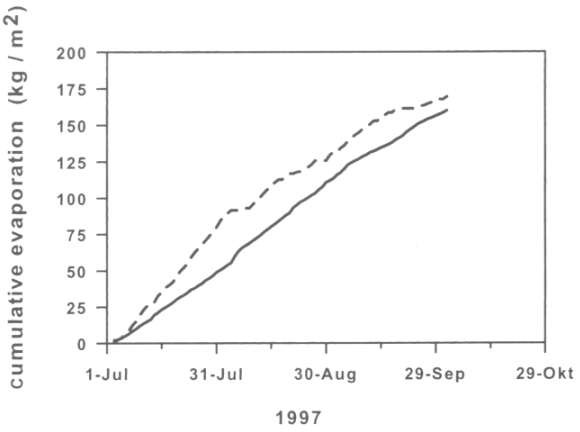

Fig. 3. Cumulative time series of evapotranspiration. (SEWAB: solid, evaporation pan: dashed). Cumulative simulated evaporation is 92 percent of pan evaporation

is left for soil moisture storage change in the simulations. For mean irish conditions the evapotranspiration from grassland amounts to about 30 percent of precipitation (Kiely, 1999). Since the evapotranspiration part is lower for our field site during the experimental period, we suggest that with increasing precipitation (above the mean value) the portion which evaporates decreases and an increasing portion goes into runoff. This is evident for soils close to saturation and close to potential evapotranspiration for most of the year.

From July to September 1997 the evaporation rate was estimated by measuring the water level in an evaporation pan. Over the whole 3-months period the simulated total evapotranspiration by SEWAB is 92 percent of pan evaporation (Fig. 3). Potential evapotranspiration at this site using Penman-Monteith is approximately 90 percent of pan evaporation. Because of the continuously moist soil conditions the evaporation is considered to be close to the maximum potential for most of the year. No further measurements of evapotranspiration are available from the field site.

5. Model validation

5.1 Simulation of the streamflow time series

Streamflow from this small catchment reacts immediately to precipitation. Sharp peaks in the time series reflect single heavy precipitation events (Fig. 4). The peaks of streamflow are simulated by inclusion of the ponding process in the model. The maximum ponding height and the time constant for the outflow from the ponding storage are determined by calibration together with an appropriate tuning of the time constant for the linear outflow from the uppermost soil layer. The model performs well for most of the year with the peaks being modelled accurately. However, the model performs less well in January 1998. This may be

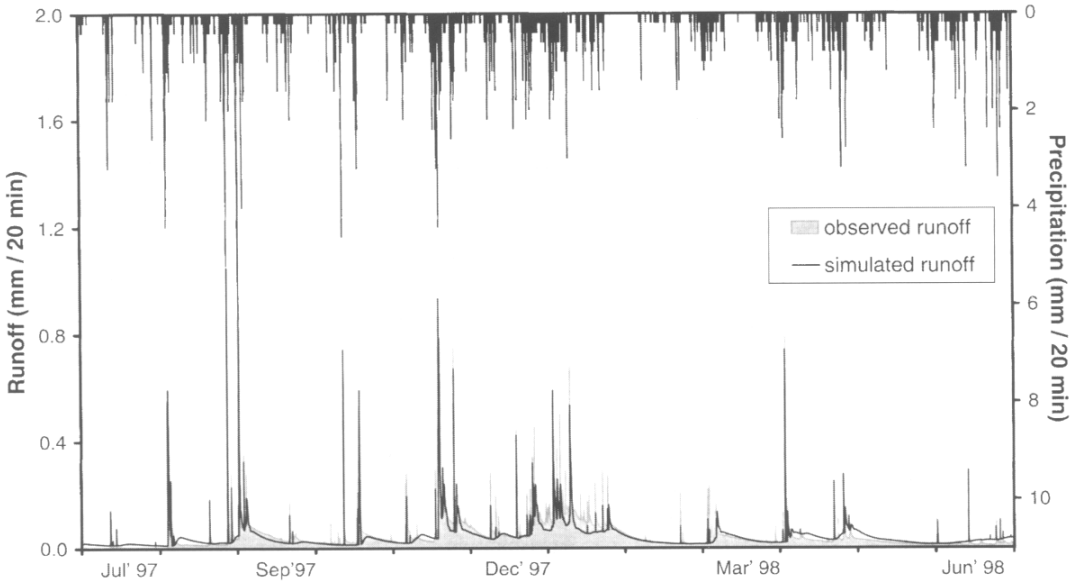

Fig. 4. Time series of simulated and observed runoff and precipitation (top axis) for the period July 1, 1997 to June 30, 1998

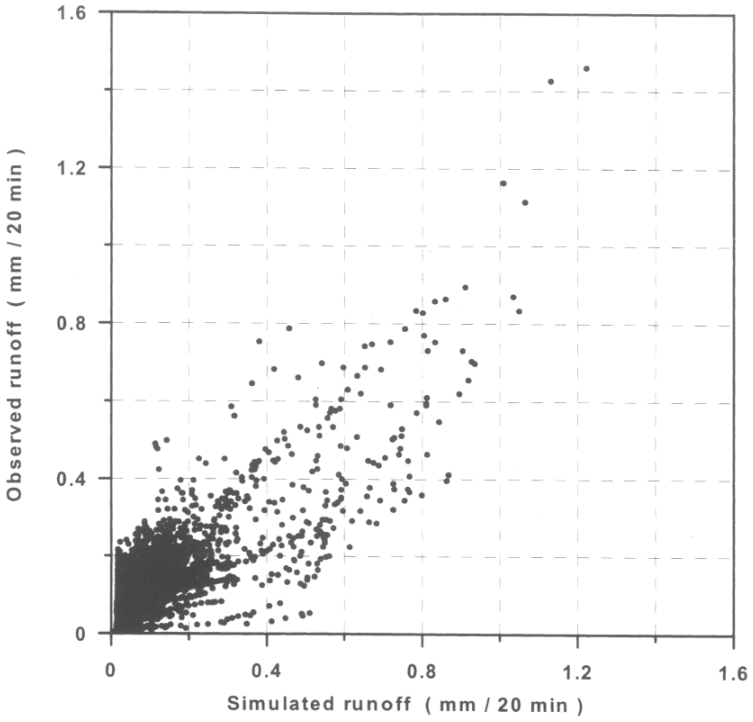

Fig. 5. Scatter diagram of runoff data. 20 min averages for the time period July, 1 1997 to June 30, 1998

due to a period of frozen ground. This period is associated with a sharp drop of the air temperature from 15 °C to 3 °C and a very cold period afterwards.

An appropriate calibration of the time constant for the slow and fast groundwater storages leads to a realistic simulation of the baseflow component of the streamflow. The transition from surface processes dominated streamflow to baseflow dominated streamflow after rainfall events is simulated rather abruptly, in contrast to the smooth change seen in the observations. However, this discrepancy becomes less important for increasing catchment areas because overland flow processes become less significant. The scatter diagram of the 20-min accumulations of simulated and observed streamflow (Fig. 5) shows no bias and no trend of a deviation over the range of flow values.

5.2 Simulation of soil moisture time series

The change in soil moisture storage contributes significantly to the surface water balance for time scales less than 1 year. The soil water content was measured by TDR at different depths during the last 130 days (February 20 to June 30, 1998) of the investigation period. The soil water content analysis is restricted to a comparison of measured and simulated time series. In Fig. 6 the simulated data represent the water content in the whole respective layer from 4 cm thickness for layer 1 to 20 cm thickness for layer 5. The depths of TDR measurements in these layers are indicated. Rainfall events and drying periods are reflected consistantly in both the measured and the simulated soil moisture time series for layers 1 to 4. Higher moisture contents at the beginning of March and at the beginning and end of April are apparent in the model and observations for layers 1 to 4. These high moisture contents are also simulated for layer 5 but are not visible in the observations. Small variations in June 1998 can be identified in both curves for layer 5. In exceptionally dry periods (around May 27) the model overestimates the moisture content. In situ observations indicate that a particular porous layer at about 10 cm depth tends to dry faster than the adjacent soil layers.

5.3 Simulation of air and soil temperature

Evaporation links the surface water and the surface energy balance. Soil water processes are also influenced by the soil temperature. Only net radiation is measured directly as one component of

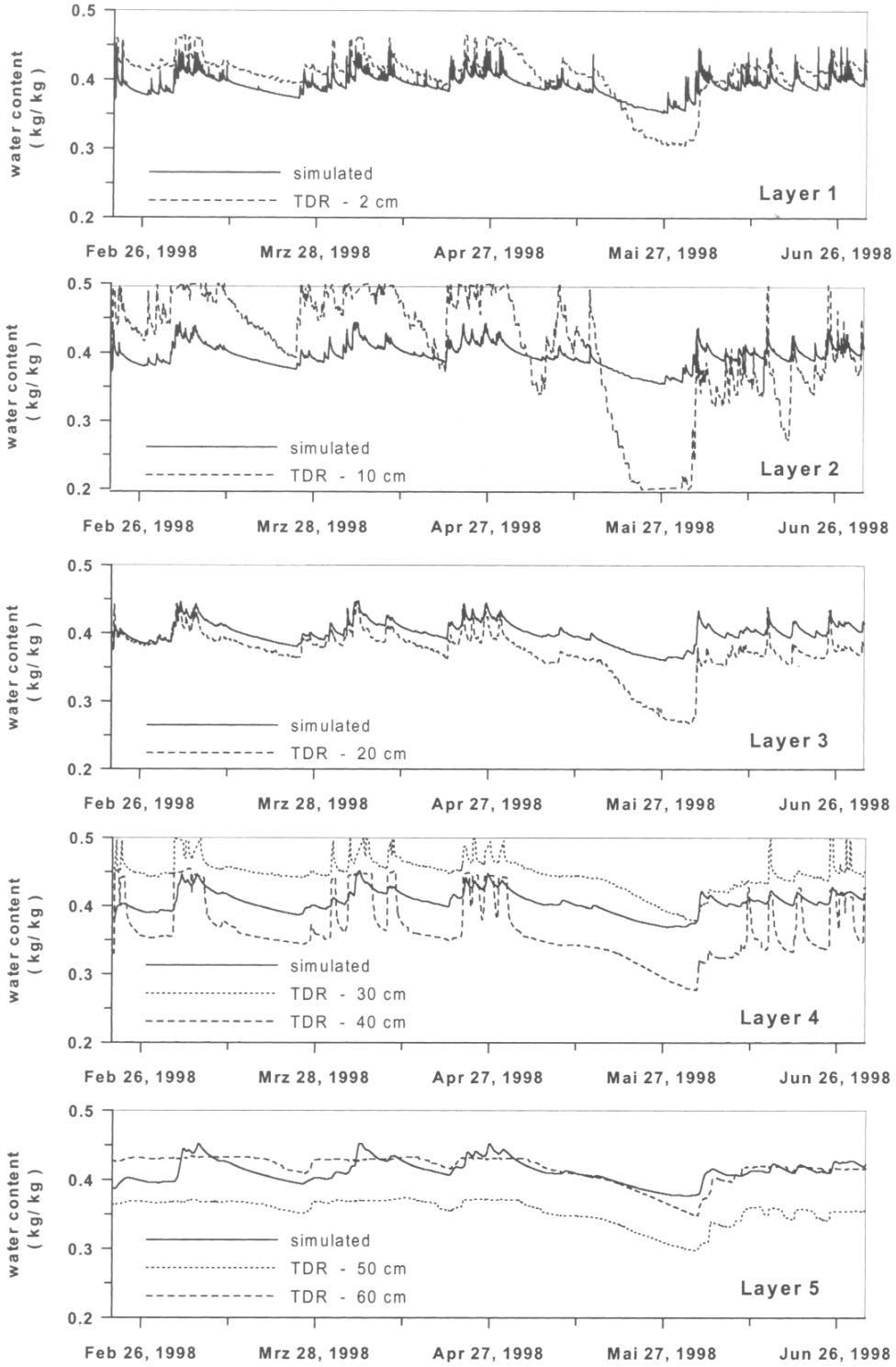

Fig. 6. Time series of measured and simulated soil moisture content for 5 soil layers for the period from February 20 to June 30, 1998

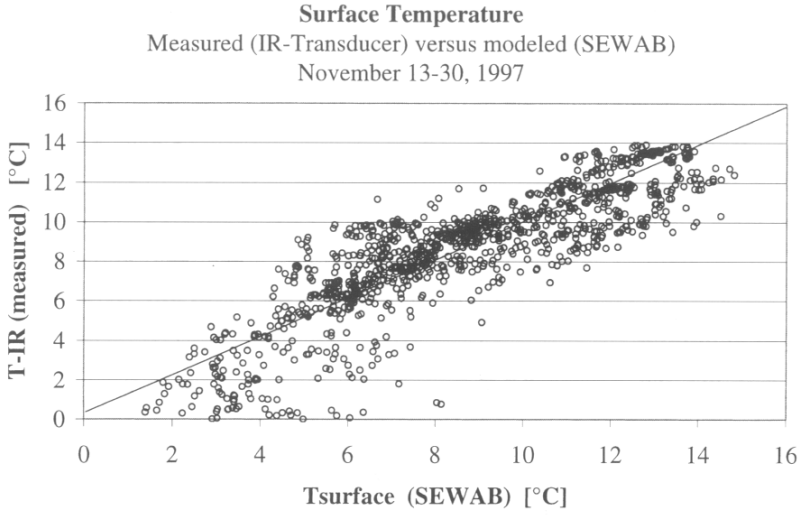

Fig. 7. Scatter diagram of the simulated and observed surface temperature. 20-min averages for the period November 13–30, 1997

the surface energy balance. Together with the observed air temperature, net radiation is provided as a forcing variable to the model. There are no direct measurements of the sensible heat flux and the soil heat flux, but these fluxes depend on the difference between the air and the surface temperature and the surface and soil temperature, respectively. While the soil temperature at 4 cm depth was measured continuously for the whole period, the surface temperature was measured by an infrared transducer from November 13 to November 30, 1997. The scatter diagram of the measured and simulated surface temperature shows no systematic deviation (Fig. 7). The model seems to slightly overestimate surface temperatures for lower values. However, the good overall correlation gives reason for the assumption that the sensible heat flux is simulated realistically. The change in soil temperature and its difference to the surface value determine the heat storage and the soil heat flux. The matching of the simulated and measured soil temperature (Fig. 8), indicates a reasonable estimation of the soil heat processes by the model when we assume that the surface temperature is adequately simulated over the whole period.

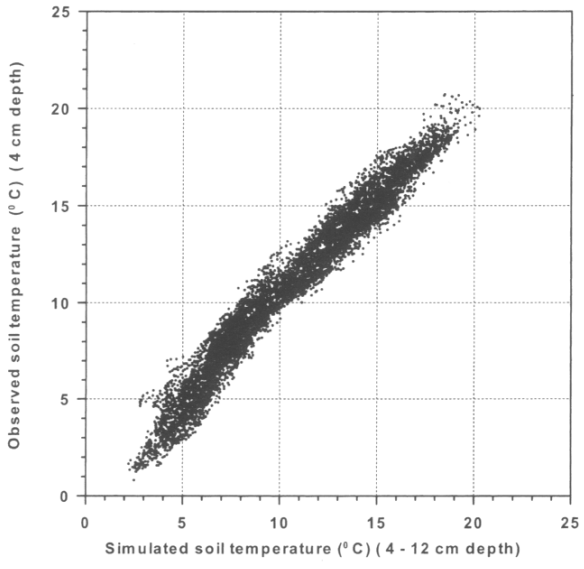

Fig. 8. Scatter diagram of the simulated and observed soil temperature. 20-min averages for the whole study period

6. The relevance of single hydrological processes

In its basic version, SEWAB generates runoff as an immediate response to saturation excess. The water which drains out of the lowest soil layer also immediately contributes to runoff. A constant value for the saturation hydraulic conductivity is applied for all soil layers. These assumptions basically determine surface runoff and baseflow generation as well as the diffusion and the gravitational drainage of water. The sensitivity of simulated streamflow to the formulation of these processes is investigated by repeating the one year simulation applying six different combinations of parameterization schemes. Case A represents the basic version of SEWAB with no particular consideration of hydrological processes, case F is the

Table 2. Case studies for different combinations of the hydrological components

	Surface runoff	Baseflow	K_{η_i}
Case A	sat. excess	free drainage	const.
Case B	sat. excess	free drainage	f(z)
Case C	sat. excess	storages	const.
Case D	ponding	storages	const.
Case E	sat. excess	storages	f(z)
Case F	ponding	storages	f(z)

simulation run described in section 5 and cases B to E represent various combinations as listed in Table 2.

As a measure of the performance of a model Nash and Sutcliff (1970) defined the efficiency R^2 by

$$R^2 = \frac{F_0^2 - F^2}{F_0^2} \tag{17}$$

with the initial variance F_0^2 defined by

$$F_0^2 = \sum_{i=1}^{n} (q_s - \bar{q}_0)^2 \tag{18}$$

where $\bar{q}_0$ is the mean discharge of n observations and

$$F^2 = \sum_{i=1}^{n} (q_s - q_0)^2 \tag{19}$$

the sum of squared deviations between simulated (q_s) and observed (q_0) discharge values. The efficiency and the square correlation are a function of the integration time. For times larger than the residence time of the water in the catchment these quantities should not depend on the particular model physics. Figure 9 shows the efficiency and the square correlation as a function of the integration time for all six cases of Table 2. The time period ranges from the measurement averaging period of 20 min over 1, 3, 6 and 12 hours to 1, 2, 3, 5, 10 and 30 days.

For an averaging period $\bar{T}$ of more than 10 days all simulations have little error. During this time period almost all the rainfall has entered the river and the single hydrological process is insignificant. However, even for such a relatively long period (with regard to the catchment size) case F shows the highest efficiency and correlation while case A appears to have the lowest performance.

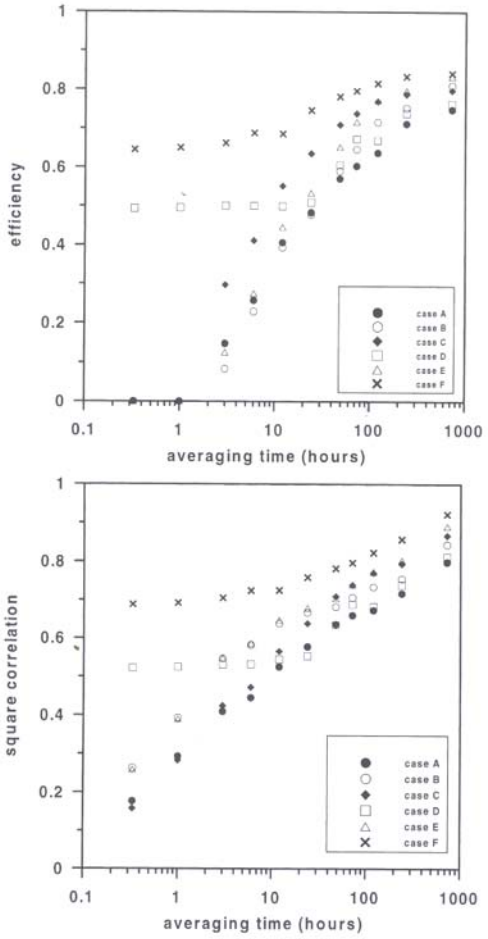

Fig. 9. Efficiency and square correlation as a function of the averaging time for six combinations of the hydrological components

For $\bar{T} > 1$ day the better performance of case E compared to case D indicates that a depth dependent saturation hydraulic conductivity is more relevant than the ponding process. At time scales less than 12 hours ponding is the most relevant process (cases D and F) while for all other cases the efficiency decreases rapidly. Cases D and F differ with regard to the vertical profile of the saturation hydraulic conductivity. For K_{η_i} varying with depth substantial improvement is obvious for all $\bar{T}$ when combined with the ponding process and the baseflow storages.

The main results of the comparison are:

- case F which includes ponding, baseflow storage compartments and a depth dependent saturation hydraulic conductivity performs best for all averaging periods
- the ponding process is essential for averaging periods of less than 12 hours
- a depth dependent saturation hydraulic conductivity improves the simulation in any case
- the baseflow storages improve the simulation in any case

7. Summary

Hydrological processes of soil water movement are added to the 1-dimensional atmospheric land surface scheme SEWAB. Ponding and infiltration are explicitly described to account for fast responses of the surface runoff to single precipitation events. Baseflow is simulated as the sum of the subsurface runoff and the outflow from a fast and slow water storage which are filled by Darcian flow from the lowest soil layer. A depth dependent saturation hydraulic conductivity accounts for a varying pore size.

The parameterization schemes describing the hydrological processes are calibrated with respect to streamflow from a small grassland catchment in Ireland. The calibration is performed for a six month period from July to December 1997 by tuning parameters manually, until simulated and observed streamflow coincide. Streamflow data from January to July 1998, soil moisture measurements, surface temperature and soil temperature for shorter periods are used for validation purposes. A comparison between simulated and observed soil water content at various depths indicates reasonable agreement in general but an overestimation by the model during exceptionally dry periods. Differences also result from the model characteristic of assuming one particular soil type for the whole column while in situ observations show layers of different porosity. Rainfall events and drying periods are reflected consistantly in both the simulated and measured soil moisture time series.

With the net radiation given as a forcing variable the similarity of the modelled and observed surface and soil temperature indicates a reasonable estimation of the surface energy balance components by the model.

This paper is based on the assumption that a sound parameterization of runoff generation is essential to realistic simulate evapotranspiration (Koster et al., 2000). The intention is to validate the runoff generation process in SEWAB on small temporal and spatial scales as they are commonly applied for the validation of the evapotranspiration. We have chosen a very small catchment which can be considered homogeneous with respect to vegetation, soil type and forcing variables to minimize the uncertainty of spatial inhomogeneity. The discharge from this small catchment responds immediately to single precipitation events. This behaviour is simulated by including ponding as an additional process into the LSS. For temporal scales greater than about 12 hours, however, this seems to be less relevant than the vertical profile of the saturation hydraulic conductivity. For temporal scales greater than about 10 days the particular hydrological process is irrelevant because this period exceeds the usual residence time of the water in the catchment.

Acknowledgements

We thank Corinna Moehrlen of University College Cork for her support during the field experiment and data analysis and the two anonymous reviewers for helpful remarks.

References

Benoit R, Pellerin P, Kouwen N, Ritchie H, Donaldson N, Joe P, Soulis ED (2000) Toward the use of coupled atmospheric and hydrologic models at regional scales. Mon Wea Rev 128: 1681–1706

Beven K (1984) Runoff production and flood frequency in catchments of the order n: an alternative approach. In: Gupta VK et al. (eds) Scale problems in hydrology. Dordrecht, Holland: D. Reidel Publishing Company, pp 107–131

Bonan GB (1996) A land surface model (LSM version 1.0) for ecological, hydrological, and atmospheric studies: technical description and user's guide, NCAR Technical Note, NCAR/TN-417+STR, National Center for Atmospheric Research, Boulder, Colorado, USA

Chen T, Henderson-Sellers A, Milly P, Pitman A, Beljaars A, Abramopoulos F, Boone A, Chang S, Chen F, Dai Y, Desborough C, Dickinson R, Dümenil L, Ek M, Garrat J, Gedney N, Gusev Y, Kim J, Koster R, Kowalczyk E, Laval K, Lean J, Lettenmaier D, Liang X, Mahfouf J, Mengelkamp H-T, Mitchell K, Nasanova O, Noilhan J, Polcher J, Robock A, Rosenzweig C, Schaake J, Schlosser C, Schulz J-P, Shao Y, Shmakin A, Verseghy D, Wetzel P, Wood E, Xue Y, Yang Z-L, Zeng Q (1997) Cabauw experimental results from the Project for Intercomparison of Land-

surface Parameterization Schemes (PILPS). J Climate 10: 1194–1215
Clapp RB, Hornberger GM (1978) Empirical equations for some hydraulic properties. Water Resour Res 14: 601–604
Deardorff JW (1978) Efficient prediction of ground surface temperature and moisture with inclusion of a layer of vegetation. J Geophys Res 83: 1889–1903
Dickinson RE (1984) Modeling evapotranspiration for three-dimensional global climate models, climate processes and climate sensitivity. (Geophysical Monograph, 29) Maurice Ewing 5: 58–72
Dümenil L, Todini E (1992) A rainfall-runoff scheme for use in the Hamburg climate model. In: O'Kane JP (ed) Advances in theoretical hydrology. A tribute to James Dooge. (European geophysical society series on hydrological sciences, 1) Amsterdam: Elsevier pp 849–859
Francini M, Pacciani M (1991) Comparative analysis of several conceptual rainfall-runoff models. J Hydrol 122: 161–219
Graham LP, Bergström S (2000) Land surface modelling in hydrology and meteorology – lessons learned from the Baltic Basin. Hydrol Earth Sys Sci 4(1): 13–22
Habets F, Etchevers P, Golaz C, Leblois E, Ledoux E, Martin E, Noilhan J, Ottle C (1999) Simulation of the water budget and the river flows of the Rhone basin. J Geophys Res 104(D24): 31145–31172
Hagemann S, Dümenil L (1999) Application of a global discharge model to atmospheric model simulations in the BALTEX region. Nordic Hydrology 30: 209–230
Hall FR (1968) Base-flow recessions – a review. Wat Resour Res 4(5): 973–983
Henderson-Sellers A, Pitman A, Love P, Irranejad P, Chen T (1995) The project for intercomparison of land-surface parameterization schemes (PILPS): Phases 2 and 3. Bull Amer Meteor Soc 94: 489–503
Hillel D (1982) Introduction to Soil Physics. San Diego: Academic Press, Inc, p 364
Kiely G, Albertson JD, Parlange MB (1998) Recent trends in diurnal variation of precipitation at Valentia on the west coast of Ireland. J Hydrol 207: 270–279
Kiely G (1999) Climate change in Ireland from precipitation and streamflow observations. Adv Wat Resour 23(2): 141–152
Koster R, Milly PCD (1997) The interplay between transpiration and runoff formulations in land surface schemes used with atmospheric models. J Climate 10: 1578–1591
Koster R, Suarez MJ, Ducharne A, Stieglitz M, Kumar P (2000) A catchment based approach to modeling land surface processes in a GCM. Part 1: Model structure. J Geophys Res (in print)
Lobmeyr M, Lohmann D, Ruhe C (1999) An application of a large scale conceptual hydrological model over the Elbe region. Hydrol Earth Sys Sci 3(3): 363–374
Lohmann D, Nolte-Holube R, Raschke E (1996) A large-scale horizontal routing model to be coupled to land surface parameterization schemes. Tellus 48A: 708–721
Lohmann D, Lettenmaier DP, Liang X, Wood EF, Boone A, Chang S, Chen F, Dai Y, Desborough C, Dickinson RE, Duan Q, Ek M, Gusev YM, Habets F, Irannejad P, Koster R, Mitchell KE, Nasonova ON, Noilhan J, Schaake J, Schlosser A, Shao Y, Shmakin AB, Verseghy D, Warrach K, Wetzel P, Xue Y, Yang ZL, Zeng QC (1998) The project for intercomparison of land-surface parameterization schemes (PILPS) phase 2(c) Red-Arkansas River basin experiment: 3. Spatial and temporal analysis of water fluxes. Global and Planetary Change 19: 161–179
Mahrt I, Pan H (1984) A two-layer model of soil hydrology. Bound-Layer Meteor 29: 1–20
Mengelkamp H-T, Warrach K, Raschke E (1999) SEWAB – a parameterization of the Surface Energy and Water Balance for atmospheric and hydrologic models. Adv Wat Resour 23: 165–175
Mengelkamp H-T, Warrach K, Ruhe C, Raschke E (2001) Simulation of runoff and streamflow on local and regional scales. Meteorol Atmos Phys 76: 107–117
Mölders N, Raabe A (1997) Testing the effect of a two-way-coupling of a meteorological and a hydrological model on the predicted local weather. Atmos Res 45: 81–107
Nash JE, Sutcliffe JV (1970) River flow forecasting through conceptual models, Part 1 – a discussion of principles. J Hydrol 10: 282–290
Noilhan J, Planton S (1989) A simple parameterization of land surface processes for meteorological models. Mon Wea Rev 117: 536–549
Peters-Lidard CD, Zion MS, Wood EF (1997) A soil-vegetation-atmosphere transfer scheme for modelling spatially variable water and energy balance processes. J Geophys Res 102(D4): 4303–4324
Richtmeyer RD, Morton KW (1967) Difference methods for initial-value problems. New York: Interscience Publishers, 406 pp
Stull B (1988) An introduction to boundary layer meteorology. Dordrecht: Kluwer Academic Publishers, pp 666
Warrach K, Mengelkamp H-T, Raschke E (1999) Runoff parameterization in a SVAT scheme: sensitivity tests with the model SEWAB. Regionalization in Hydrology, IAHS publ 254: 123–130
Wood EF, Lettenmaier DP, Zartarian VG (1992) A land-surface hydrology parameterization with subgrid variability for general circulation models. J Geophys Res 97(D): 2717–2728
Wood EF, Lettenmaier DP, Liang X, Lohmann D, Boone A, Chang S, Chen F, Dai Y, Dickinson RE, Duan Q, Ek M, Gusev YM, Habets F, Irannejad P, Koster R, Mitchell KE, Nasonova ON, Noilhan J, Schaake J, Schlosser A, Shao Y, Shmakin AB, Verseghy D, Warrach K, Wetzel P, Xue Y, Yang Z-L, Zeng Q-C (1998) The project for intercomparison of land-surface parameterization schemes (PILPS) phase 2(c) Red-Arkansas basin experiment: 1. Experiment description and summary intercomparisons. Global and Planetary Change 19: 115–135

Author's address: Heinz-Theo Mengelkamp, Kirsten Warrach, Institute for Atmospheric Physics, GKSS Research Center Geesthacht, Max-Planck-Staqsse, D-21502 Geesthacht, Germany (e-mail: mengelkamp@gkss.de); Gerard Kiely, Dept. of Civil and Environmental Engineering, University College Cork, Cork, Ireland.